IEEE Access
Multidisciplinary | Rapid Review | Open Access Journal

Received August 9, 2017, accepted September 5, 2017, date of publication September 19, 2017, date of current version October 12, 2017.

Digital Object Identifier 10.1109/ACCESS.2017.2754325

Stress Assessment Based on Decision Fusion of EEG and fNIRS Signals

FARES AL-SHARGIE[1], (Member, IEEE), TONG BOON TANG[1], (Member, IEEE), AND MASASHI KIGUCHI[2]

[1]Center of Intelligent Signal and Imaging, Department of Electrical and Electronic Engineering, Universiti Teknologi PETRONAS, Perak 32610, Malaysia
[2]Research and Development Group, Hitachi Ltd., Saitama 350-0395, Japan

Corresponding author: Tong Boon Tang (tongboon.tang@utp.edu.my)

The work was supported by the Ministry of Higher Education, Malaysia, under HiCOE fund scheme.

ABSTRACT Fusion of electroencephalography (EEG) and functional near infrared spectroscopy (fNIRS) is an emerging approach in the field of psychological and neurological studies. We developed a decision fusion technique to combine the output probabilities of the EEG and fNIRS classifiers. The fusion explored support vector machine as classifier for each modality, and optimized the classifiers based on their receiver operating characteristic curve values. EEG and fNIRS signal were acquired simultaneously while performing mental arithmetic task under control and stress conditions. Experiment results from 20 subjects demonstrated significant improvement in the detection rate of mental stress by $+7.76\%$ ($p < 0.001$) and $+10.57\%$ ($p < 0.0005$), compared with sole modality of EEG and fNIRS, respectively.

INDEX TERMS Stress, neuroimaging, decision fusion.

I. INTRODUCTION

Stress is a growing problem in our society and is part of our daily life. We spend most of our time as adults at workplace. Extended periods of high workload and time pressure contribute to increased level of mental stress [1], [2]. Conventionally, mental stress is evaluated by using subjective questionnaires, cortisol level and other physiological signals (i.e. heart rate, blood pressure and skin conductance) [1]. Such methods known to be affected by circadian rhythm and cardiovascular diseases [3], [4]. As mental stress is originated from the amygdala, it is desirable to study the stress effects on brain activities and measure them noninvasively using modern neuroimaging modalities [5].

Functional magnetic resonance imaging (fMRI) and positron emission tomography (PET) have gained a reputation of having high spatial resolution (a few millimeter). These techniques measure the hemodynamic induced by regional changes in neural activities, based on the principle of neurovascular coupling. Nevertheless, they have limitations in their temporal resolution (a few seconds to several minutes) and are susceptive to movement artifacts [5]. Moreover, subjects need to remain still during fMRI/PET measurements [6]. Electroencephalography (EEG), on the other hand, measures the neural activities as electrical potentials with temporal resolution in the order of a few milliseconds, which makes it suitable for measuring dynamic cortical changes during daily workplace activities [7]. Unlike fMRI and PET, modern EEG hardware is light-weighted and portable enough to allow unconstrained full-body movements. Few studies have used EEG to classify mental stress from resting state [8], [9] as the EEG has traditionally been thought to possess poor spatial resolution (a few mm to one cm) and be highly prone to motion artifacts [10]. Functional Near-Infrared Spectroscopy (fNIRS) offers a better immunity against motion artifacts, and is particularly suitable for clinical and non-clinical studies of large population. The fNIRS detects the neural activities of the brain by measuring the change in concentration of oxygenated hemoglobin (O_2Hb) and deoxygenated hemoglobin (HHb) in the cortex [11], [12]. The fNIRS achieves some middle ground in terms of spatial and temporal resolutions between EEG and MRI techniques, and have been shown to be consistent with fMRI and EEG results [13]–[15].

Fusion of EEG and fNIRS has the advantages of allowing human cortical activities to be measured without major constraints on the mobility of subjects, and complement of each other in the temporal and spatial resolution. It can be achieved at either feature level or decision level [16], [17]: at feature level, techniques such as joint Independent Component Analysis (jICA) and Canonical Correlation

Analysis (CCA) [16], [18] exploit main features from each modality to derive a coherent description of the targeted model (e.g. workplace stress) across all subjects; at decision level, the targeted model is modeled by local classifiers for each modality and the local decisions are then combined to improve the overall performance [19].

In this work, we introduce a decision-level fusion approach to integrate two local decisions according to the operating points on their receiver operating characteristic (ROC) curves. The ROC curves are generated based on the decisions from support vector machine (SVM) classifiers. The overall results show that the proposed decision fusion approach achieves a significant improvement over individual EEG/fNIRS classification performance. In the next section, we describe about the participant selection, protocol development, and the sets of EEG and fNIRS signals used. We then explain the methods of data processing for statistical analysis, classification and fusion. Section III reports the results and Section IV provides a discussion before the conclusion in Section V.

II. METHODOLOGY

A. PARTICIPANTS

Twenty-two male, right-handed adults (age 22 $\pm$ 2 years) volunteered to participate in the study. All participants were explained about the study and gave their written consents prior to the experiment. The study conformed to the recommendations by the local ethics review committee at the Universiti Teknologi PETRONAS, and in accordance with the Declaration of Helsinki. None of the participants had a history of neurological or cardiological disorder. Each participant was seated comfortably in a room with good air condition before and during the experiment to avoid any environmental stress. Additionally, all participants received brief introduction about the task and instructed to avoid any body/head movement, deep breathing and to keep calm during the entire measurements.

B. STRESS TASK AND PROCEDURES

The task performed in this study was based on the Montreal Imaging Stress Task (MIST) described in detail in [20]. The task designed and presented in MATLAB with Graphical User Interface (GUI). It involved 3-single digit integer (from 0 to 9) and used the addition (+) or subtraction (−) operands (for example, 2−3+9). The answers were presented in the sequence of 0 to 9 and participant had to select the right answer by doing single-click using the mouse. The task was performed in three phases; training, control and stress phase. Each of the phase is described as follows.

Training Phase: Participants practiced the arithmetic task for a total duration of five minutes. In this phase, the percentage of correct answers and the time taken by each individual were recorded. Two subjects with poor performance, i.e. score <70% correct, were dropped from this study. The average recorded time would be reduced by 10% in the stress phase as time pressure (stressor) for each participant.

Control Phase: A custom-made EEG+fNIRS probe holder was attached to the participant's head and signals were simultaneously recorded for a total duration of five minutes. In this phase, each participant was instructed to solve the arithmetic problems as fast as he could, but without any time limit per question. At the end of the phase, participants filled up self-report questionnaire about workload using *NASA-Task Loading Index* (NASA-TLX) [21].

Stress Phase: Simultaneous measurements of EEG+fNIRS were recorded for a total duration of five minutes. In this phase, each participant solved the arithmetic problems under time pressure (the average time taken during the training phase with a reduction of 10%). In addition, feedbacks of answer (''correct'', ''incorrect'' or ''timeout'') were displayed on the computer monitor to further induce stress in participants. Performance indicators (one for the participant and one for the peer that was fixed at 90% accuracy) were also displayed on the monitor to introduce peer pressure. At the end of the stress phase, participants filled up another NASA-TLX self-report questionnaire about the task loading.

Fig. 1 summarizes the overall experimental procedures. A block design that incorporated both the control and the stress tasks was used in the presented study. A total of 10 blocks were used (five blocks in the control phase and five blocks in the stress phase). In both phases (control and stress), the arithmetic task in each block was displayed for 30 seconds followed by 20 seconds rest. During the 20 s rest, participants were instructed to focus on a fixation cross with black background to sustain their attention to the monitor display. The order of the task conditions (control/stress) was assigned randomly with an equal number of participants for each sequence. The reaction time and the accuracy in answering the questions under the control and the stress phases were recorded as behavioral data and used for analysis.

C. SUBJECTIVE ASSESSMENT

The subjective assessment of mental stress was conducted using questionnaire NASA-TLX [21]. Participants were asked to evaluate their mental workload after performing the control task as baseline and after the simultaneous measurements of the EEG and fNIRS under the stress condition. The NASA-TLX relies on subjects' consciously perceived experience with regards to the effort requirement and difficulty of task. Compare to other subjective measures of workload, NASA-TLX has the advantage of being quick and simple to administer. The NASA-TLX is divided into six subscales, namely mental demand (MD), physical demand (PD), temporal demand (TD), own performance (OP), effort (EF) and frustration (FR). Each of these six subscales scores from '1' to '20' based on the performance of participants. The overall scores about workload were then weighted (weighted workload, WWL) to 100 and used for evaluation.

D. SIMULTANEOUS MEASUREMENT OF EEG+fNIRS

A custom-made probe holder/cap of optical topography system (OT-R40, Hitachi Medical Corporation, Japan) and EEG

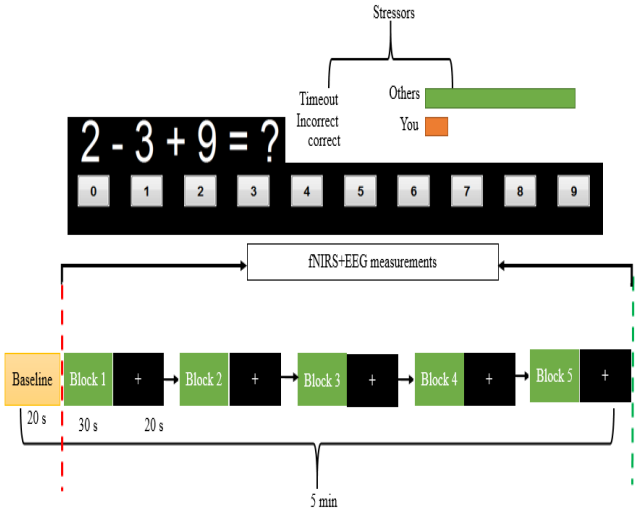

FIGURE 1. Schematic of the experimental procedure for mental stress study. The tasks in the control as well as the stress phase were presented in block design. In each phase, there were five blocks. Mental arithmetic in each block was allocated for 30 s followed by 20 s rest.

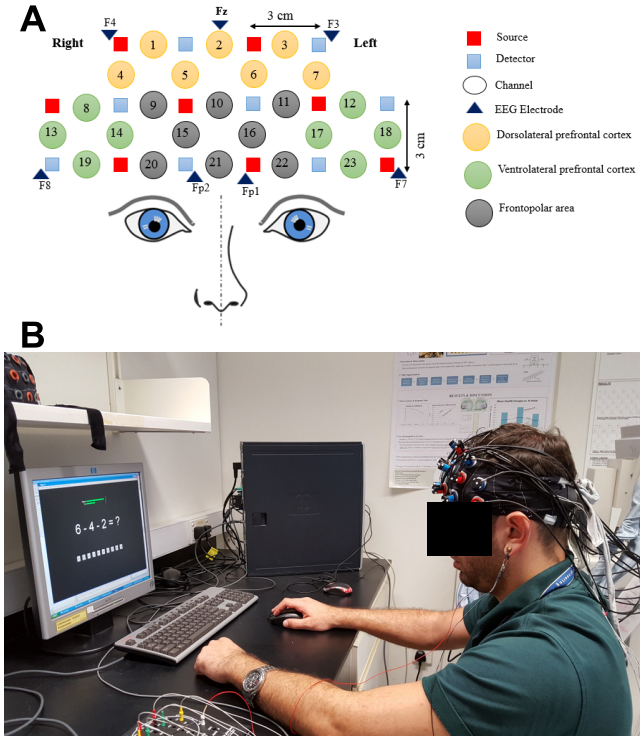

FIGURE 2. Probe setting and schematic arrangement points. (A) Location of the fNIRS probe array/optodes (red=sources; blue= detectors) and EEG electrodes according to the international 10-20 system. Channels (numbered from 1 to 23) were measured at three lateral PFC subregion. Each subregion/anatomical area represented by different color. There were a total of twenty three fNIRS channels and 7-EEG electrode. (B) Overall experiment set-up and task presentation.

(BrainMaster 24E system) was used for the EEG+fNIRS measurements. The EEG system was equipped with seven-active electrodes (FP1, FP2, F3, F4, Fz, F7 and F8) and sampled at 256 Hz. The light sources of the fNIRS system consisted of continuous laser diodes with two wavelengths, 695 nm and 830 nm. The detected light was sampled every 100 ms. A total of 16 optodes: 8-sources and 8-detectors were placed over the PFC area between locations FP1/2-F3/4-F7/8 thus covering the Frontopolar area (FPA, Ch 9-11, 15, 16, 20-22), Dorsolateral (DLPFC; 1-7) and Ventrolateral (VLPFC; 8, 13, 14, 19, 12, 17, 18, and 23), using the anatomical landmarks provided by the international 10-20 system. The distance between pairs of source and detector probes was set to 3 cm as demonstrated in Fig. 2(A). The measurement area between a pair of source-detector probes was defined as a channel (Ch). As a result, 23 optical channels were recorded. The arrangement and appearance of the probe array/electrode in experiment set up is shown in Fig. 2. We controlled the simultaneous measurement of EEG+fNIRS using MATLAB. Two triggers were sent, one through the serial port and the other one through the parallel ports to mark the start and the end of the task in each block of the mental arithmetic task in the fNIRS and EEG systems, respectively. The physical connections were achieved by three links. The first connection was the communication link between the EEG amplifier and the main measurement controller (a desktop was used in this study for control signals and stimulus display) via a 3 m USB cable with choke for EEG data acquisition. The second communication link was to send markers to the EEG amplifier. The Discovery 24E had two channels (Channel 23 and 24) available to receive markers from an external source, in this case the main measurement controller. In order to create the link, the EEG amplifier was connected through a special cable (381-071) to a PC printer port. The cable was provided by BrainMaster and was optically isolated for safety and noise immunity. In order to send the marker to the EEG amplifier, we used the MATLAB data acquisition Toolbox to write a signal (either '1' as Start or '0' as End) to Channel 23/24 of EEG amplifier. The third communication link was between the OT-R40 and the main measurement controller. This was achieved using the RS232 interface of the OT-R40 and a USB-to RS232 converter. In this study, we have chosen 'F9' to mark the start, and 'F7' to mark the end of a block.

E. EEG AND fNIRS DATA PROCESSING

EEG data were preprocessed using a custom script as well as the EEGLAB toolbox [22]. Using a third order Butterworth filter, the data were bandpass-filtered between 0.5 Hz and 30 Hz to eliminate high frequency physiological noise. Eye-blinks and eye-movements were identified using Independent component analysis (ICA) technique and removed manually. EEG data were decomposed into seven independent components, and the one which described prefrontal eye blink artifacts was manually rejected [18]. Baseline correction was done by taking the average of first 300 ms before the task, and had it removed from all subsequent data points. Then EEG data were re-referenced to linked-earlobes (A1+A2). Clean EEG signals were then

decomposed into delta frequency band signals (0-4 Hz), theta frequency band signals (4-8 Hz), alpha frequency band signals (8-16 Hz), and beta frequency band signals (16-32 Hz) using wavelet transform (WT) [23]. We used the WT due to its ability in describing time-frequency features that are highly correlated with stress levels [20]. Only data from alpha frequency band were considered in this study due to its relatively higher sensitivity to stress exposure [20]. Using a time-sliding window of 500 ms, the mean power values of alpha frequency band signals were extracted and used as features for EEG assessment.

Similarly, the raw fNIRS data were transformed to the product of optical path length and concentration of oxygenated and de-oxygenated hemoglobin using modified Beer-Lambert approach [24]. The ΔO_2Hb and ΔHHb were preprocessed to remove low-frequency physiological change and high-frequency systemic noise using a custom code as well as plug-in analysis software Platform for Optical Topography Analysis Tool (POTATo) [25]. The signals in all the channels were filtered with a third order band-pass Butterworth filter between 0.012 and 0.8 Hz. In order to exclude high frequency artifacts, a moving average was calculated using a time window of 5 s. We used the moving average due to its ability in removing spurious artifacts in continuous signals. A period from the start of the task to the end period of the task condition (a duration of 30 s) was defined as one single analysis block. Each task block was then baseline-corrected by subtracting the average value of the pre-task period from that of all subsequent data points in the task period. Following the baseline correction, the five blocks were averaged into a single block of 30 s to find the average hemodynamic response. In the present study, we used the mean ΔO_2Hb measured during the arithmetic task in the control and stress conditions as an index of cortical activity. Similarly as the case in EEG, features were extracted from the mean change concentration of oxygenated hemoglobin (ΔO_2Hb) using a moving timing-window of 500 ms. The selection of 500 ms time-window was to synchronize the features of the two modalities. We chose the O_2Hb as an index because it has a stronger correlation with fMRI BOLD (blood-oxygenation level-dependent) signals than HHb [26].

F. STATISTICAL ANALYSIS

To reveal the differences in brain responses between control and stress groups in the subjective assessment as well the simultaneous measurement of EEG+fNIRS, we analyzed the differences between them in channel/electrode basis using matched-pairs t-test. In each electrode/channel, the differences were considered statistically significant if the p value is less than 0.001, $p < 0.001$.

G. CLASSIFICATION PERFORMANCE

To classify the EEG and fNIRS signals, support vector machine (SVM) classifiers were used. SVM is a supervised machine learning classifier defined by a hyperplane [27]. The SVM is one of the most commonly used classifier in the field of pattern recognition, biomedical and neuroscience studies due its potential in modeling linear as well as more complex decision boundary. We used the LIBSVM software to build the SVM classifier with Radial Basis Function (RBF) kernels to nonlinearly map data onto a higher dimension space [28].

Each data feature from the EEG and the fNIRS was segmented randomly into ten segments or 10-fold cross-validations. Nine segments were used for training of the SVM classifier, and the other one segment used for testing. We repeated this process for ten times until each segment had been used for testing and training. The optimum kernel parameters gamma γ and the penalty factor C were determined over a space that maximized the accuracy in each fold. The SVM classifier was evaluated on each segment (cross-validation) in terms of accuracy, sensitivity, specificity and area under the receiver operation characteristic (ROC) curve. The overall performance of the EEG and fNIRS classifiers from the ten cross validations were then evaluated by the mean ROC curves.

H. DECISION FUSION OF EEG AND fNIRS SIGNALS

The decision fusion was achieved by fusing the outputs/decisions from two local classifiers (SVMs), one for EEG signals and the other for fNIRS signals. Each classifier was calibrated based on the optimal operating points of EEG and fNIRS ROC curves. The global classifier used in this study for decision fusion is also SVM with RBF kernels.

Let the output of individual local classifier be denoted as u_k, (EEG: $k = 1$; fNIRS: $k = 2$), where $u_k = 0$, if the decision of kth classifier is H_0 (no-stress) and $u_k = 1$ if the decision of classifier is H_1 (stress). The decision of classifier u_k depends on the features vectors x_k, $k = 1, 2$.

$$u_k = \alpha_k(x_k) \begin{cases} 0, & \text{classifier } k \text{ decides } H_0 \text{ (no stress)} \\ 1, & \text{classifier } k \text{ decides } H_1 \text{ (stress)} \end{cases} \quad (1)$$

where α_1 and α_2 are sets of threshold value of EEG and fNIRS local classifiers respectively. The performance characteristics of classifier $k$specified by $P(u_k = 1|H_j)$ where $P(u_k = 1|H_0) = P_{fk}$ *is* the probability of false positives, and $P(u_k = 1|H_1) = P_{dk}$ *is* the probability of true positives. Using these probabilities, the likelihood ratio value of a binary decision variable may be obtained by:

$$\lambda_{decision} = \frac{P(u_k|H_1)}{P(u_k|H_0)} = \left(\frac{P_{dk}}{P_{fk}}\right)^{u_k} \left(\frac{1-P_{dk}}{1-P_{fk}}\right)^{1-u_k} \quad (2)$$

The decision at the fused level depends only on local decisions and their probability of true positive P_{dk} and false positive P_{fk}. Since individual classifiers are based on different modalities, the two decisions assumed to be statistically independent. The fusion likelihood ratio could then be generated using the following form:

$$\lambda_{fusion}(u_1, u_2) = \prod_{k=1}^{2} \left(\frac{P_{dk}}{P_{fk}}\right)^{u_k} \prod_{k=1}^{2} \left(\frac{1-P_{dk}}{1-P_{fk}}\right)^{1-u_k} \quad (3)$$

The optimal fused decision rule uses the fusion likelihood ratio as a classification decision variable and then compares it to threshold β for decision u according to the following:

$$u = F(u_1, u_2) = H\left(\lambda_{fusion} - \beta\right) \tag{4}$$

where H is the Heaviside function. By varying the threshold β value (corresponding to different decision rules), N number of operating points were derived for the fused ROC curve. The probability of true positive rate and false positive rates for decision-fused classifier operating points could then be calculated based on the following equations:

$$Pd_{fusion}(\beta) = \sum_{\lambda_{fusion} \geq \beta} P\left(\lambda = \lambda_{fusion} | H_1\right) \tag{5}$$

$$Pf_{fusion}(\beta) = \sum_{\lambda_{fusion} \geq \beta} P\left(\lambda = \lambda_{fusion} | H_0\right) \tag{6}$$

The entire decision-fused ROC curve obtained by deriving a series of $Pk_{fusion}(\beta)$ using multiple combinations of operating points on EEG-/fNIRS-based local classifier ROC curves.

III. RESULTS

Experiment result showed that the performance of subjects decreased with stress, accuracy score in answering the arithmetic questions correctly was <40%, as expected. The results of subjective rating about workload, as measured by NASA-TLX across the control and the stress conditions for all subscales, are presented in Table 1. The weighted workloads (WWLs) in the control and stress conditions were 22.2 and 75.4, respectively. Based on the responses from the participants, frustration (FR) subscale was the most significant factor (t-value = 7.62) followed by own performance (OP). Overall, there was a significant difference between the subjective score from the control and the stress condition across all the subjects and the NASA-TLX subscales. Based on the t and p values as summarized in Table 1, the experiment results confirm the success of moderate stress inducement in every subject.

TABLE 1. Comparison of NASA-TLX subscales means ± se after control and stress conditions of the arithmetic task.

NASA-TLX	Control	Stress	T-test result	
			t-value	p-value
MD	20.0±7.6	75.0±4.7	6.30	<0.0001
PD	25.0±8.4	77.0±6.3	6.41	<0.0001
TD	23.0±6.6	78.0±4.5	6.31	<0.0001
OP	85.0±6.3	20.0±3.1	7.41	<0.0001
EF	30.0±4.5	68.0±2.3	5.81	<0.0001
FR	32.0±3.2	88.0±1.2	7.62	<0.0001
WWL	22.2±2.5	75.4±3.7	6.21	<0.0001

Abbreviations: MD, mental demand; PD, physical demand; TD, temporal demand; OP, own performance; EF, effort; FR, frustration; WWL, weighted workload; MW, mental workload; T-test analysis; SE, standard error.

The result of EEG showed that alpha rhythm fluctuated from control to stress condition in all the participants.

TABLE 2. Statistical analysis of O_2Hb and EEG alpha rhythm.

Channel	t-value (SD)	p-value (<)	Channel	t-value (SD)	p-value (<)
1	5.3±0.62	0.0002	16	6.1±0.64	0.0001
2	4.3±0.56	0.0005	17	2.8±0.44	0.0573
3	3.1±0.53	0.0012	18	2.1±0.93	0.0665
4	5.6±0.51	0.0001	19	5.1±0.12	0.0001
5	5.7±0.62	0.0001	20	5.2±0.22	0.0001
6	6.0±4.30	0.0002	21	5.3±0.55	0.0002
7	2.5±0.71	0.0610	22	5.0±0.75	0.0005
8	6.4±0.34	0.0001	23	2.5±0.66	0.0606
9	5.2±0.44	0.0005	F4	5.7±0.31	0.0001
10	6.5±0.74	0.0001	Fz	4.8±0.22	0.0002
11	6.5±0.71	0.0001	F3	4.9±0.65	0.0005
12	2.2±0.73	0.0620	F8	5.6±0.31	0.0001
13	5.2±0.11	0.0002	F7	4.6±0.61	0.0005
14	4.8±0.14	0.0005	Fp1	5.5±0.73	0.0002
15	6.6±0.71	0.0001	Fp2	5.4±0.41	0.0001

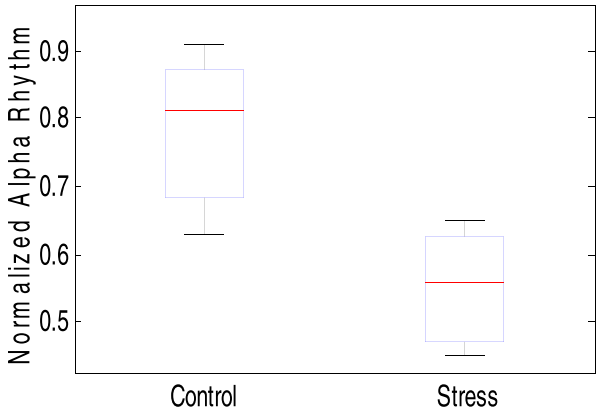

FIGURE 3. Normalized EEG alpha power values at the control and stress phase.

The fluctuations/decrease in the EEG alpha rhythm was found across all the electrodes in the entire PFC area. The overall statistical analysis (average: t and p values) of each EEG electrode is summarized in Table 2, with F4, F8 and FP1 showing the highest t-values. The normalized alpha power values in all the electrodes at the control and at the stress phases are presented as boxplot in Fig. 3.

Similarly, the results of fNIRS demonstrated a significant increase in the oxygenation level (the O_2Hb change) with a corresponding decrease in HHb during the control arithmetic task, in relative to the pre-task baseline over the entire PFC (except Ch-18 and Ch-23). As expected, under stress condition the O_2Hb changes decreased or absence in most of the PFC regions relative to pre-task, on average (except at Ch-7 and Ch-12). The overall average time-course of O_2Hb (red line) and HHb (blue line) changes under control and stress conditions are shown in Fig. 4 and Fig. 5, respectively. As the O_2Hb signals highly reflect the cortical activities, we limited our analysis in this work to their response.

The focus of this study is to investigate on the cortical responses to working memory task (mental arithmetic) under

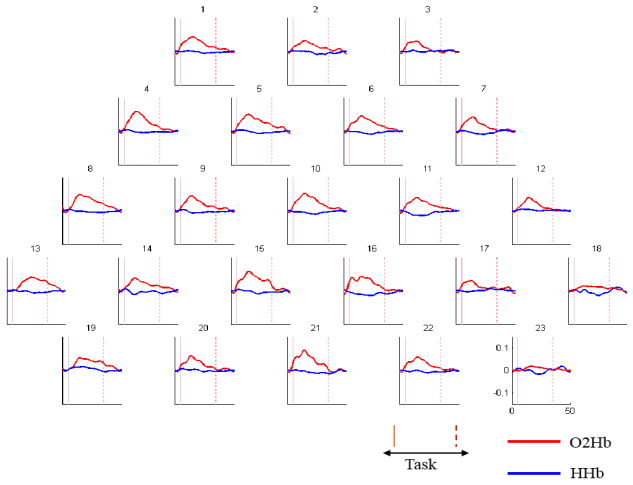

FIGURE 4. Average time-course of oxygenated (red line) and de-oxygenated (blue line) hemoglobin concentration changes during the arithmetic task at control condition across all the subjects for 23-channels. Two markers were used to mark the start of the task (vertical red line) and the end of the task (vertical red-dashed line) in every channel.

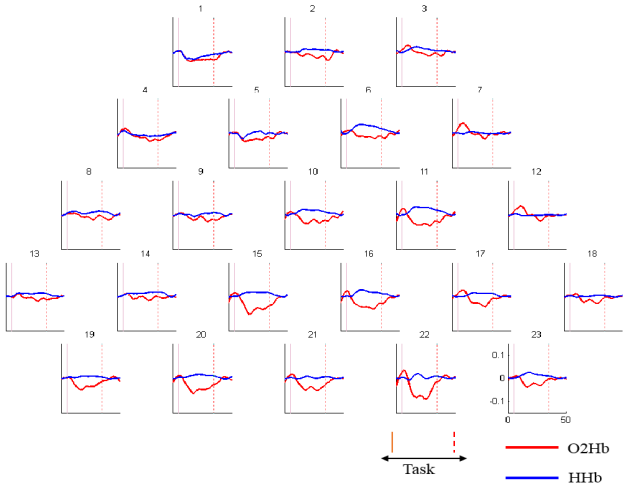

FIGURE 5. Average time-course of oxygenated (red line) and de-oxygenated (blue line) hemoglobin concentration changes during the arithmetic task at stress condition across all the subjects for 23-channels. Two markers were used to mark the start of the task (vertical red line) and the end of the task (vertical red-dashed line) in every channel.

control and stress conditions. We thus conducted a statistical analysis between the two groups. The experimental results revealed significant decreases in the O_2Hb changes from control condition in Fig.4 to stress condition in Fig.5 in most regions of the PFC areas (except at Ch-7, Ch-12, Ch-17, Ch-18 and Ch-23). The experimental results in Fig.4 and Fig.5 further showed that stress is a sub-region specific, and the left PFC area is less affected by mental stress. Table 2 summaries the statistical analysis of all the subjects and channels represented by t and p values with their standard deviations (SD). The lowest standard error across all channels is located at the right ventrolateral PFC, i.e. Ch-13, Ch-14 and Ch-19, indicating that this sub-region is most susceptive to mental stress, across all the participants.

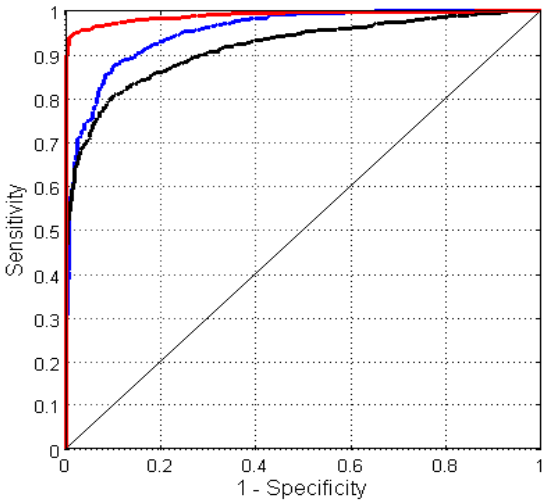

FIGURE 6. ROC curve of EEG (blue line), $fNIRS_1$ (black line) and EEG+$fNIRS_1$ (red line). $fNIRS_1$ comprised channels Ch-5, Ch-6, Ch-13, Ch-18, Ch-15, Ch-16 and Ch-2.

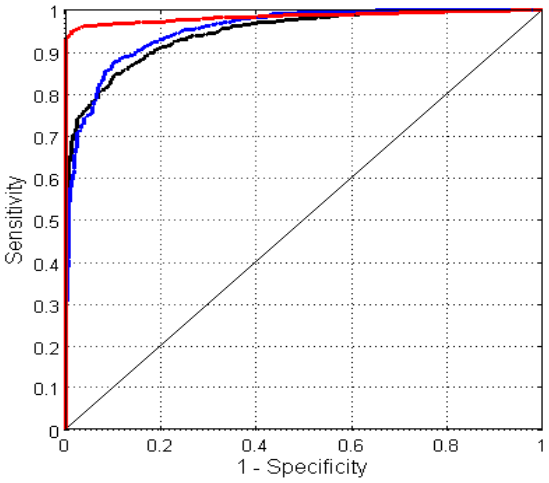

FIGURE 7. ROC curve of EEG (blue line), $fNIRS_2$ (black line) and EEG+$fNIRS_2$ (red line). $fNIRS_2$ comprised channels Ch-1, Ch-3, Ch-19, Ch-23, Ch-20, Ch-22 and Ch-2.

The classification results of EEG modality, fNIRS modality and fusion of EEG+fNIRS are shown by their ROC curves. Features from the seven electrodes (FP1, FP2, Fz, F3, F4, F7 and F8) were used for evaluating EEG modality and for fusion with the $fNIRS_1$ and $fNIRS_2$. The $fNIRS_{(1,2)}$ channel selection was based on t-value approach (channels with the highest t-value) as well as the lateralizing channels from each subregion of the PFC areas (within the right and left: DLPFC, VLPFC and FPA). The first $fNIRS_1$ channels were Ch-5, Ch-6, Ch-13, Ch-18, Ch-15, Ch-16 and Ch-2. The second $fNIRS_2$ channels were Ch-1, Ch-3, Ch-19, Ch-23, Ch-20, Ch-22 and Ch-2. Fig.6 and Fig.7 show the ROC curves of individual EEG, $fNIRS_1$, $fNIRS_2$, fusion of EEG+$fNIRS_1$ and fusion of EEG+$fNIRS_2$. The black line shows the result from $fNIRS_{(1,2)}$, blue line shows the result from EEG and the red line shows the result of fusing EEG+$fNIRS_{(1,2)}$, respectively.

The average classification performance (obtained from 20 subjects) of sole EEG, sole $fNIRS_1$, fusion of EEG+$fNIRS_1$, sole $fNIRS_2$ and fusion of EEG+$fNIRS_2$ in the form of accuracy, sensitivity, specificity and area under the ROC curves are summarized in Table 3. Decision fusion shows improvements in the classification accuracy in the range of +7.76% ($p<0.001$) to +10.57% (0.0005) compare to sole EEG and sole $fNIRS_{(1,2)}$ respectively. Similar improvements were found in the classification sensitivity, specificity and in the area under ROC curves in the range of +3.45% to +11.65%. Using two sample t-test, fusion of EEG+$fNIRS_{(1,2)}$ significantly improves the overall classification performance in all the metrics with $p < 0.001$.

TABLE 3. Classification performance of eeg, fnirs and eeg+fnirs.

Modality	Accuracy (%)	Sensitivity (%)	Specificity (%)	AROC (%)
EEG	88.69	87.60	89.70	95.10
$fNIRS_1$	84.76	82.50	87.00	91.50
$fNIRS_2$	87.00	84.40	89.70	94.40
$fNIRS_1$+ $fNIRS_2$	85.88	83.45	88.35	92.95
EEG+ $fNIRS_1$	96.42	94.80	97.90	98.80
EEG+ $fNIRS_2$	96.48	95.40	97.50	98.30
EEG+ $fNIRS_{(1,2)}$	96.45	95.10	97.70	98.55
Improvement over EEG	+7.76	+7.50	+8.00	+3.45
Improvement over fNIRS	+10.57	+11.65	+9.35	+5.60

IV. DISCUSSION

This study investigated decision fusion of EEG and fNIRS signals for discriminating between responses to arithmetic task under control and stress conditions. The EEG and fNIRS data were acquired simultaneously while participants solving the arithmetic tasks. The behavioral responses as well as the subjective evaluation demonstrated that all participants experienced stress while solving the task with the introduction of stressors. Measurement from EEG provides data on the electrical activity whereas fNIRS provides data on the hemodynamics of the cortex. These two neuroimaging modalities complement each other in quality (time/spatial resolution) as well as in the quantity (information). Thus, fusing decisions from these measuring responses enhance the detection rate of mental stress.

The experimental results show that decision fusion of the EEG and the fNIRS classifier outputs improves the overall classification performance, compared to individual classifier. EEG classifier gives a mean classification accuracy, sensitivity, specificity and area under the ROC curve of 88.69%, 87.6%, 89.7% and 95.1%, respectively. Similarly, the results from the $fNIRS_{(1,2)}$ classifiers give a mean classification accuracy, sensitivity, specificity and area under the ROC curve of 85.88%, 83.45%, 88.35% and 92.95%, respectively. On the other hand, fusions of EEG+$fNIRS_{(1,2)}$ demonstrated significant improvements over individual EEG/$fNIRS_{(1,2)}$ classifier with mean classification accuracy, sensitivity, specificity and area under the ROC curves of 96.45% ($p<0.001$), 95.10% ($p<0.001$), 97.70% ($p<0.0005$) and 98.55%,($p<0.001$), respectively. The percentage of improvements achieved in this study is in the range of 3.45% to 11.65% in all the four metrics namely; accuracy, sensitivity, specificity and area under the ROC curve. As expected, the improvements on the classification performance support the hypothesis of fusing decisions from EEG and fNIRS may provide complementary information for better stress detection. Proper selection of data processing and analysis is crucial to optimize the fusion. Unlike feature-level fusion reported in our previous study [18], decision fusion of ROC classifiers is more flexible. The technique allows the parameter optimization of classifier to be performed independently for each modality, and subsequently refines the classification results from each modality.

The improvements in our fusion is also consistent with previous EEG+fNIRS studies [17], [29]–[36]. These previous studies were based on motor imagery tasks which are relatively simple and stable. Additionally, these studies used large number of EEG and fNIRS channels which usually require longer time for preparation, and are more likely to cause discomfort. For example, Fazli et al. proposed a hybrid sensory motor rhythm combined 24 fNIRS channels and 37 EEG electrodes. The researcher used a meta-classifier to combine the output probability of the individual classifier-modality. The results showed that the simultaneous measurement of the EEG+fNIRS can significantly improve the classification accuracy of the motor imagery by an average of +5% [17]. Lee et al. [30] used similar number of channels/electrodes and demonstrated that bimodal EEG+fNIRS signals increase the classification performance by +10% for the motor imagery task. Morioka *et al.* [34] used 49 channels and 64 EEG electrodes and reported that the hybrid system of EEG+fNIRS improved the spatial attention decoding accuracy by +8%. Blokland *et al.* [33] recently examined the principle of combining these modalities in patients with tetraplegia. The researcher used 2 channels with 8 electrodes but reported poor improvements in the accuracy of brain switch control, −1%. Up to date, our study is the first investigation about fusing EEG+fNIRS at decision level to study complex neurological behaviors such mental stress. The highest improvement of 11.65% in our study supports the efficiency of the proposed fusion.

V. CONCLUSION

This study proposed a novel decision fusion of EEG+fNIRS for improving the detection rate of mental stress. The fusion was based on fusing two SVM classifier decisions based on their ROC curves. The proposed fusion improves the classification accuracy in detecting stress by +10.57%, and +7.76% compared to sole fNIRS and sole EEG, respectively. Similar improvements were found in the sensitivity, specificity and in the area under the ROC curves. Our study showed that, albeit with less number of electrodes/channels, the improvements of fusion were significant, therefore suggesting EEG+fNIRS as a potential tool of stress measurements on the PFC area.

REFERENCES

[1] A. Alberdi, A. Aztiria, and A. Basarab, "Towards an automatic early stress recognition system for office environments based on multimodal measurements: A review," *J. Biomed. Informat.*, vol. 59, pp. 49–75, Feb. 2016.
[2] N. Sharma and T. Gedeon, "Modeling observer stress for typical real environments," *Expert Syst. Appl.*, vol. 41, no. 5, pp. 2231–2238, 2014.
[3] R. Den, M. Toda, S. Nagasawa, K. Kitamura, and K. Morimoto, "Circadian rhythm of human salivary chromogranin A," *Biomed. Res.*, vol. 28, no. 1, pp. 57–60, 2007.
[4] F. Custodis, J.-C. Reil, U. Laufs, and M. Böhm, "Heart rate: A global target for cardiovascular disease and therapy along the cardiovascular disease continuum," *J. Cardiol.*, vol. 62, no. 3, pp. 183–187, 2013.
[5] K. Dedovic, C. D'Aguiar, and J. C. Pruessner, "What stress does to your brain: A review of neuroimaging studies," *Can. J. Psychiatry*, vol. 54, pp. 6–15, Jan. 2009.
[6] J. A. Levine, I. T. Pavlidis, L. MacBride, Z. Zhu, and P. Tsiamyrtzis, "Description and clinical studies of a device for the instantaneous detection of office-place stress," *Work*, vol. 34, no. 3, pp. 359–364, 2009.
[7] C. M. Michel and M. M. Murray, "Towards the utilization of EEG as a brain imaging tool," *Neuroimage*, vol. 61, no. 2, pp. 371–385, 2012.
[8] N. Sharma and T. Gedeon, "Objective measures, sensors and computational techniques for stress recognition and classification: A survey," *Comput. Methods Programs Biomed.*, vol. 108, no. 3, pp. 1287–1301, Dec. 2012.
[9] L. Xin, C. Zetao, Z. Yunpeng, X. Jiali, W. Shuicai, and Z. Yanjun, "Stress state evaluation by an improved support vector machine," *J. Med. Imag. Health Informat.*, vol. 5, pp. 742–747, Apr. 2015.
[10] C. Babiloni, V. Pizzella, C. D. Gratta, and A. Ferretti, and G. L. Romani, "Fundamentals of electroencefalography, magnetoencefalography, and functional magnetic resonance imaging," *Int. Rev. Neurobiol.*, vol. 86, pp. 67–80, Apr. 2009.
[11] F. F. Jöbsis, "Noninvasive, infrared monitoring of cerebral and myocardial oxygen sufficiency and circulatory parameters," *Science*, vol. 198, no. 4323, pp. 1264–1267, 1977.
[12] A. Villringer and B. Chance, "Non-invasive optical spectroscopy and imaging of human brain function," *Trends Neurosci.*, vol. 20, no. 10, pp. 435–442, Oct. 1997.
[13] M. L. Schroeter, T. Kupka, T. Mildner, K. Uludağ, and D. Y. von Cramon, "Investigating the post-stimulus undershoot of the BOLD signal—A simultaneous fMRI and fNIRS study," *NeuroImage*, vol. 30, pp. 349–358, Apr. 2006.
[14] L. Li, P. Du, T. Li, Q. Luo, and H. Gong, "Design and evaluation of a simultaneous fNIRS/ERP instrument," in *Proc. Biomed. Opt.*, 2007, p. 643429-6.
[15] M. Strait and M. Scheutz, "What we can and cannot (yet) do with functional near infrared spectroscopy," *Frontiers Neurosci.*, vol. 8, pp. 1–12, May 2014.
[16] N. M. Correa, Y. O. Li, T. Adali, and V. D. Calhoun, "Canonical correlation analysis for feature-based fusion of biomedical imaging modalities and its application to detection of associative networks in schizophrenia," *IEEE J. Sel. Topics Signal Process.*, vol. 2, no. 6, pp. 998–1007, Dec. 2008.
[17] S. Fazli *et al.*, "Enhanced performance by a hybrid NIRS–EEG brain computer interface," *NeuroImage*, vol. 59, no. 1, pp. 519–529, 2012.
[18] F. Al-Shargie, T. B. Tang, and M. Kiguchi, "Assessment of mental stress effects on prefrontal cortical activities using canonical correlation analysis: An fNIRS-EEG study," *Biomed. Opt. Exp.*, vol. 8, no. 5, pp. 2583–2598, 2017.
[19] B. V. Dasarathy, *Decision Fusion*. Los Alamitos, CA, USA: IEEE Comput. Soc. Press, 1994.
[20] F. Al-Shargie, M. Kiguchi, N. Badruddin, S. C. Dass, A. F. M. Hani, and T. B. Tang, "Mental stress assessment using simultaneous measurement of EEG and fNIRS," *Biomed. Opt. Exp.*, vol. 7, pp. 3882–3898, Oct. 2016.
[21] S. G. Hart and L. E. Staveland, "Development of NASA-TLX (task load index): Results of empirical and theoretical research," *Adv. Psychol.*, vol. 52, pp. 139–183, Dec. 1988.
[22] A. Delorme and S. Makeig, "EEGLAB: An open source toolbox for analysis of single-trial EEG dynamics including independent component analysis," *J. Neurosci. Methods*, vol. 134, no. 1, pp. 9–21, Mar. 2004.
[23] T. Gandhi, B. K. Panigrahi, and S. Anand, "A comparative study of wavelet families for EEG signal classification," *Neurocomputing*, vol. 74, no. 17, pp. 3051–3057, 2011.
[24] A. Sassaroli and S. Fantini, "Comment on the modified Beer-Lambert law for scattering media," *Phys. Med. Biol.*, vol. 49, p. N255, Jul. 2004.
[25] S. Sutoko *et al.*, "Tutorial on platform for optical topography analysis tools," *Neurophotonics*, vol. 3, no. 1, p. 010801, 2016.
[26] H. Sato *et al.*, "A NIRS-fMRI investigation of prefrontal cortex activity during a working memory task," *NeuroImage*, vol. 83, pp. 158–173, Dec. 2013.
[27] V. N. Vapnik and V. Vapnik, *Statistical Learning Theory*, vol. 1. Hoboken, NJ, USA: Wiley, 1998.
[28] C.-C. Chang and C.-J. Lin, "LIBSVM: A library for support vector machines," *ACM Trans. Intell. Syst. Technol.*, vol. 2, no. 3, pp. 27:1–27:27, 2011.
[29] S. Ge *et al.*, "A brain-computer interface based on a few-channel EEG-fNIRS bimodal system," *IEEE Access*, vol. 5, pp. 208–218, 2017.
[30] M.-H. Lee, S. Fazli, J. Mehnert, and S.-W. Lee, "Subject-dependent classification for robust idle state detection using multi-modal neuroimaging and data-fusion techniques in BCI," *Pattern Recognit.*, vol. 48, no. 8, pp. 2725–2737, 2015.
[31] V. Kaiser *et al.*, "Cortical effects of user training in a motor imagery based brain-computer interface measured by fNIRS and EEG," *NeuroImage*, vol. 85, pp. 432–444, Jan. 2014.
[32] X. Yin *et al.*, "A hybrid BCI based on EEG and fNIRS signals improves the performance of decoding motor imagery of both force and speed of hand clenching," *J. Neural Eng.*, vol. 12, no. 3, p. 036004, 2015.
[33] Y. Blokland *et al.*, "Combined EEG-fNIRS decoding of motor attempt and imagery for brain switch control: An offline study in patients with tetraplegia," *IEEE Trans. Neural Syst. Rehabil. Eng.*, vol. 22, no. 2, pp. 222–229, Mar. 2014.
[34] H. Morioka *et al.*, "Decoding spatial attention by using cortical currents estimated from electroencephalography with near-infrared spectroscopy prior information," *NeuroImage*, vol. 90, pp. 128–139, Apr. 2014.
[35] A. P. Buccino, H. O. Keles, and A. Omurtag, "Hybrid EEG-fNIRS asynchronous brain-computer interface for multiple motor tasks," *PLoS ONE*, vol. 11, p. e0146610, Jan. 2016.
[36] K.-S. Hong and M. J. Khan, "Hybrid brain-computer interface techniques for improved classification accuracy and increased number of commands: A review," *Frontiers Neurorobot.*, vol. 11, pp. 1–27, Jul. 2017.

FARES AL-SHARGIE was born in Al Dhale, Yemen in 1984. He received the B.S. and M.S. degrees in electronics majoring in bio-instrumentation from Multimedia University, Malaysia, and the Ph.D. degree in electrical engineering from Universiti Teknologi PETRONAS, Malaysia. His current research interests include the assessment of mental stress via, EEG, fNIRS neuroimaging modality, and cortisol level. He is a member of the Society of Functional Near-Infrared Spectroscopy.

TONG BOON TANG was born in Johor, Malaysia, in 1976. He received the B.Eng. degree (Hons.) and the Ph.D. degree from the University of Edinburgh. He is currently an Associate Professor with the Universiti Teknologi PETRONAS. His research interests are in biomedical instrumentation, from device and measurement to data fusion. He received the Lab on Chip Award in 2006 and the IET Nanobiotechnology Premium Award in 2008. He is an Associate Editor of the *Journal of Medical Imaging and Health Informatics*, and the Vice Chair of the IEEE Circuits and Systems Society Malaysia Chapter.

MASASHI KIGUCHI has studied various mental problems, including working memory, emotions, depression, blood flow, mental stress, and has been taking the lead in the development of new techniques for observing brain activities to open new research fields and in basic studies for putting them to practical use.